Narrowband coherent Rayleigh-Brillouin scattering from gases confined by a high-intensity optical lattice

Barry M. Cornella, Sergey F. Gimelshein, Taylor C. Lilly, and Andrew D. Ketsdever

Phys. Rev. A **87**, 033825 — Published 22 March 2013

DOI: 10.1103/PhysRevA.87.033825

Narrowband coherent Rayleigh-Brillouin scattering from gases confined by a high-intensity optical lattice

Barry M. Cornella[*] and Sergey F. Gimelshein[†]

ERC Inc., Edwards AFB, CA 93524, USA

Taylor C. Lilly[‡]

University of Colorado, Colorado Springs, CO, USA

Andrew D. Ketsdever[§]

Air Force Research Laboratory, Edwards AFB, CA 93524, USA

Molecular nitrogen at 0.8 atm and 300/500 K and methane at 0.8 atm and 300 K were subjected to optical lattices formed by narrowband, 532 nm, laser pulses with intensities on the optical axis near, but below, the gas ionization limit. A third pulse was introduced to experimentally probe the response, as a function of the lattice velocity, of the gas to the deep monochromatic potential wells formed by the lasers. Coherent Rayleigh-Brillouin scattering (CRBS) line shapes were recorded and compared to numerically predicted magnitudes of the density perturbations induced in the gas. Both experimental results and those from direct simulation Monte-Carlo simulations show deviation from previously published low intensity CRBS line shape models. The deviation indicates a similar trend, as a function of lattice velocity, as that relating to previously published energy and momentum transfer calculations for high intensity lattices. Furthermore, the deviation indicates a maximum intensity at which current CRBS theory is valid.

[*] Coop Researcher
[†] Senior Research Engineer
[‡] Assistant Professor, Dept. of Mechanical and Aerospace Engineering
[§] Senior Research Engineer, AFRL/RQRS

I. INTRODUCTION

The analysis of laser-gas interactions within pulsed optical lattices has proven to be a useful tool in gas diagnostics. Coherent Rayleigh scattering (CRS) and coherent Rayleigh-Brillouin scattering (CRBS) typically utilize low intensity (relative to ionization or dissociation) laser pulses to form a light interference pattern referred to as an optical lattice [1]. Gas atoms or molecules within the optical lattice, in turn, experience a force that tends to push them towards area of lowest potential. As a result, the optical potential pattern creates periodic density perturbations in a gas sample with a periodicity on the order of the laser wavelength [2]. By scattering a probe laser off the density grating formed by the lattice the returned signal can be spectroscopically connected to the thermodynamic properties and velocity distribution of the gas sample [3, 4]. A visual representation of this process can be found in FIG. 1. The coherent scatter from forced density gratings offers significant increases in signal strength over spontaneous processes [5]. CRS and CRBS, as gas diagnostic techniques, have proven their use for yielding information about a gas, such as temperature [6, 7] and bulk viscosity [8, 9]. To yield this information, the necessary intermediate step is predicting the strength of the density perturbation for a given set of laser and gas parameters. Because CRS and CRBS typically use low intensity pulses, where the potential well depth is small compared to the thermal energy of the gas, the effects of the lattice on the gas manifests itself as a small perturbation to the equilibrium state, deemed to have negligible effect on the state of the gas. Operating in this perturbative regime has allowed analytical models to be developed for the collisionless/weakly collisional cases of CRS [3] and for the collisional case of atomic and molecular CRBS [10].

In an effort to achieve even higher signal strengths, higher intensity lattices with deeper potential wells may be used to increase the density perturbation. However, deep optical potential wells ($> 0.1\ kT$) can have a significant impact on the velocity distribution of the gas as the molecules transition from being perturbed by, to becoming trapped within, the well. Experimental and numerical studies have been performed for the low density case of CRS at high intensities [11] and indicate a power narrowing in the CRS line shape due to the trapped molecules within the potential field. However, the high density case of CRBS at high intensity has yet to be explored due to the complexity of modeling the interaction process as it pertains to the influence of intermolecular collisions.

This study investigates CRBS line shapes within high intensity laser fields. CRBS measurements in this high intensity regime offer the advantage of signal levels orders of magnitude higher than those obtained in the perturbative regime. A narrowband CRBS experiment is performed and compared to the low intensity kinetic line

shape model for molecular nitrogen and methane. Because developing a high intensity CRBS kinetic model offers unique and decided challenges, due to significant deviation from equilibrium, a complimentary statistical approach has been used to predict the CRBS line shape. The direct simulation Monte Carlo (DSMC) method has previously been applied to CRBS spectra in the low intensity regime [12] and is used here to compare to the experiment. Furthermore, the DSMC approach can yield information regarding the impact of a high intensity field on the affected gas inaccessible to the experiment, to further study the gas dynamics within the CRBS process at high intensities. For instance, the use of DSMC allows for numerical sampling of local gas temperature and velocity distribution within the high intensity CRBS interaction. Preliminary results for high intensity CRBS in nitrogen at 300 K can be found in [13]. The presented results were expanded to include various gas species and initial temperatures.

II. THEORETICAL FRAMEWORK

Detailed theory for the effect of an optical lattice on a collisional gas and the scattering of a probe beam off the resulting density perturbation formed by that interaction can be found in [3, 14-17]. Because the laser wavelength is on the order of the gas mean free path, a kinetic treatment is needed. For low intensity cases, line shape models have been developed using approximations to the one-dimensional Boltzmann equation and yield a theoretical expression for the CRBS power spectrum. For atomic species, these models are based on the linearized Bhatnagar-Gross-Krook (BGK) approximations. In order to accommodate internal degrees of freedom, the Wang-Chang-Uhlenbeck (WCU) approximations are used for molecular species. These approximations, however, are limited to predicting kinetic flows where the deviation from equilibrium is small. Thus, existing line shape models are ineffective in predicting the CRBS line shape in a regime where the effect on the gas is cannot be considered perturbative, as with high intensity laser pulses (for instance, $>1\text{x}10^{16}$ W/m^2), and the influence of intermolecular collisions is strong [18].

An alternative approach to modeling kinetic flow parameters through an approximation to the Boltzmann equation is the direct simulation of gas particles. This study uses a direct simulation Monte Carlo (DSMC) technique, which is a statistical approach to the solution of the Boltzmann equation. The DSMC technique simulates particle trajectories and, statistically, the effect of collisions in physical space to model gas flows. As a result, a complete flow field can be modeled at the kinetic level. While all simulation methods make some set of

assumptions based on the phenomenon under investigation, the DSMC approach makes generally less restrictive assumptions than those found in the previously published simplified models. Common assumptions made in the simplified models include values for hard to find gas parameters, such as bulk viscosity. The models also assume small perturbations to the equilibrium condition which limits their applicability. Contrarily, DSMC modeling makes the same assumptions as the Boltzmann equation for kinetic fluids including the existence of the molecular chaos and binary collisions. The direct simulation of fluid particles makes no presumptions on the gas velocity distribution allowing DSMC to be suitable for modeling non-equilibrium flows such as those found in high intensity optical lattices. A modified version of the DSMC code, SMILE, was used in a configuration consistent with the experiments. SMILE has been previously used in predicting CRBS line shapes in the low intensity regime [12] and is applied here to higher intensities.

The code was modified to include the force exerted on the molecules from the optical lattice. The dipole force acting on a polarizable medium in a non-uniform electric field is given by Boyd [1] as the negative gradient of the potential field, U, induced by the applied field, which can be written as

$$F = -\nabla U = \left(\frac{\alpha}{2}\right)\nabla E^2 \tag{1}$$

where α is the directionally averaged static polarizability [C m^2 V^{-1}] of the particle and E is the electric field [V m^{-1}]. For a pair of idealized anti-parallel, coherent, collimated laser pulses, the force acting on a particle within the potential region is given [12, 19] by

$$F = -\left(\frac{\alpha q}{2}\right) E_1 E_2 \, sin(qx - \Omega t) \tag{2}$$

where E_n, k_n, and ω_n, are pump 1 and 2 electric field strengths [V m^{-1}], wave number [rad m^{-1}], angular frequency [rad s^{-1}] respectively, $q=k_1-k_2$ is the lattice (interference pattern) wave number [rad m^{-1}] and $\Omega=\omega_1-\omega_2$ is the lattice angular frequency [rad s^{-1}]. Note that q and Ω define the velocity of the lattice, $\xi = \Omega/q$ [m s^{-1}]. The sign of Ω defines the direction of ξ.

The periodic nature of the dipole force induces a local area of higher density at the anti-nodes of the interference pattern. This perturbation, in turn, causes a periodic structure in the index of refraction of the gas, which is related to its density, effectively creating a grating which will scatter light. Given the CRS/CRBS experimental parameters, such as the angle of the crossing pumps and the wavelength of the lasers, the scattered light will evolve as a coherent scatter off the grating, increasing the signal significantly over a spontaneous processes [3, 4, 20]. It has been shown

that the intensity of the returned light in a CRS/CRBS experiment is proportional to the intensity of the probing light and the square of the density perturbations in the gas [21].

$$I_{sig} \propto I_{probe} \delta\rho^2 \tag{3}$$

Thus, the DSMC simulations can be compared to experimental data by relating the square of the numerically sampled density field with the acquired scattered signal intensity.

III. SIMULATION PARAMETERS

The modification to the SMILE code used a Newtonian integration scheme to approximate the dipole force given by Eq. (2) on a molecule as a temporally and spatially varying acceleration [22]. The acceleration was considered constant over the duration of a simulation time step. Time steps were therefore reduced such that the species did not traverse appreciable fractions of the laser field or temporal pulse width in one time step. The variable hard sphere (VHS) model [23] and majorant frequency scheme [24] were employed for modeling molecular collisions. The values of the VHS model parameters used in the DSMC computations can be found in [12]. The latter feature was particularly important for maintaining fidelity while reducing the time step to satisfy the laser interaction conditions. The Larsen-Borgnakke model for continuous internal energies was used to calculate rotation-translation energy transfer, with temperature-dependent relaxation numbers [25, 26]. For nitrogen and methane, vibrational relaxation at the tested temperatures is negligible. Assuming the validity of Eq. (3), the numerical simulation package was used to calculate the density perturbation created by the periodic force given by Eq. (2). As in the experiment, 0.8 atm nitrogen initially at 300 K and 500 K along with methane at 300 K were used as the test gases.

The nominal set of conditions and laser parameters were chosen to match those contained in the experiment. The nominal condition simulated a pair of 532 nm wavelength, 45 μm (FWHM), 5 ns (FWHM) pulses interacting with the test gas. Single pump energies were set to 130 mJ, 190 mJ, and 90 mJ for nitrogen (300 K and 500 K) and methane respectively. The simulation domain was modeled as axisymmetric around the optical axis of the two idealized anti-parallel, counter-propagating pulses. The lattice phase velocity in the forcing function described in Eq. (2) was varied in increments of 50 m/s through the range corresponding to the experiment. In order to cover the temporal shape of the pulses, each pulse simulation ran from $-\tau$ to $+\tau$ where τ was assumed to be 5 ns (FWHM). Therefore, the total time for each simulation was 10 ns. With an experimental interaction length of approx. 2 mm, the axial domain boundaries were considered periodic. The radial domain boundary was considered specular and

assumed to represent a sufficiently small cross-section at the center of the laser focus, such that the surrounding volume was equally affected. The domain was nominally 6.65 nm tall, in one cell, and 532 nm wide, 80 cells. The SMILE code was allowed to automatically subdivide cells for the calculation of collisions based on local flow conditions.

The first step in the simulation procedure was to populate the domain in the baseline ambient configuration with the appropriate gas properties. Flow field properties were sampled over one time step every $1/20^{th}$ of a run, $1/10^{th}$ of a pulse width, in order to yield a time-dependent evolution of the gas in the simulation domain. With approximately 7,500,000 simulated particles per sample cell, the average statistical error is estimated at approximately 0.1%. The numerical density perturbation was found by a non-linear least squares fit of the axial domain density to a cosine. The amplitude of the cosine fit was used as the magnitude of the density perturbation. As discussed above, the square of the density perturbation is proportional to the magnitude of the scattered signal. Diagrams of the simulation domain and the fitting procedure are available in ref. [12].

IV. EXPERIMENTAL SETUP

The general experimental setup was constructed after previous narrowband configurations [12, 17]. The use of all narrowband lasers for CRBS simplifies the correlation of the two pulses within their coherence distance and yields equivalent results as the use of broadband CRBS pumps. The narrowband approach, however, requires scanning of one of the pump beam's frequency to cover the desired spectral range, instead of the use of an etalon [16] for spectral resolution from a broadband return. The configuration produces the necessary deep potential wells required for this high intensity CRBS investigation, while also allowing direct comparison to the simulated condition of a single frequency optical interference pattern. A diagram of the optical configuration for this experiment can be seen in FIG. 2.

Two Q-switched, frequency doubled, injection seeded, Nd:YAG lasers, each with ~5 ns pulses, generated the two narrowband pumps with a line widths of ~90 MHz (from the manufacturer). The two pump pulses passed through a set of 500 mm focal length lenses and crossed to form the interaction region with a diameter of ~45 μm. The crossing angle was 178° ±0.5° as measured by spatial locations on the crossing lenses. A probe beam was split from pump 1, rotated in polarization orthogonal to the pump beams so not to interfere with the lattice interaction, and separately sent to the interaction region. This configuration required the signal to also be orthogonal in

polarization to the pump beams, allowing it to be extracted using a thin film polarizer. The timing of the lasers was controlled by high precision delay generators. Care was taken in matching the path length of the probe to pump 1 and determining the timing of pump 2 to ensure the all three beams arrived at the interaction region simultaneously. The coherence length of the two pulses was approximately 3 m based on the speed of light over the line width, $c/\Delta\nu$. For a path length matching to within 0.3 m, the interaction region was well within the coherence length, creating deep monochromatic potential wells. Therefore, the lattice interaction was both coherent and correlated [27].

Because the probe beam and pump 1 were degenerate, the probe beam was set to directly counter-propagate pump 1. This configuration required the scattered signal to propagate counter to pump 2, independent of the frequency difference between the two lasers. For further information on the phase matching condition, which aides beam alignment across frequency sweeping, see refs. [4, 12, 17] and the schematic in FIG. 1. The center frequency of pump 2 was varied by a voltage input to the injection seed laser allowing explicit control over the lattice velocity. The frequency was scanned such that the range of the frequency differences varied from 0 to ~5 GHz, in increments of ~15 MHz. Due to the symmetric nature of the line shapes, only the positive frequency differences were scanned to ensure consistency of the laser system over the temporal extent of the run. Small fractions of each seed laser (1064 nm) were interfered and the beat frequency measured on a fast amplified InGaAs photodiode. The measurements were taken on a 7 GHz oscilloscope, yielding a direct measurement of the frequency difference of the pumps at each increment ($\Delta\nu_{pump}=2\Delta\nu_{seed}$).

Molecular nitrogen and methane initially at 300 K were used as the test gases. Additionally, nitrogen was also tested at 500 K. In order to accommodate the higher laser intensities required in this investigation, a modification to the test gas configuration from previous setups [12] was implemented to avoid optical damage to gas cell components. Instead of the gas cell or vacuum chamber, a slow moving jet of the test gas through a vertical tube was placed at the interaction region. The flow velocity was ~0.2 m/s and the pressure within the jet was 0.8 atm (local ambient conditions). The lasers passed through the tube through a set of holes drilled perpendicular to the tube axis as shown in FIG. 3. Each pump energy was set such that the combined intensity of the pump beams was ~80% of the test gas optical ionization threshold: 130 mJ, 190 mJ, and 90 mJ for nitrogen at 300 K, 500 K and methane at 300 K respectively. The corresponding intensities were therefore well beyond the small perturbation regime for the lattice-gas interaction [11]. At each frequency point, the scattered beam was detected on a high speed GaAs photodiode and the signal averaged over 50 shots.

V. RESULTS AND DISCUSSION

The experimental and numerical results for high intensity CRBS in (a) molecular nitrogen at 300 K (b) nitrogen at 500 K and (c) methane at 300 K are shown in FIG. 4. The maxima of the experimentally recorded (averaged) scattered signal are compared to the numerically simulated density perturbations (squared). Also shown in FIG. 4 is the low intensity six-moment kinetic model calculated by Pan [10]. The results from the experiment and DSMC were normalized by area. Pan's s6 line was normalized to zero frequency difference with the DSMC results as it was easier to examine the deviation from the low intensity model. The residuals of both the experiment and DSMC against the s6 model are also shown. Scatter in the experimental data arises from laser pointing instabilities in both space and time. As seen in FIG. 4, the high intensity experiment and DSMC results are in good agreement for both tests at 300 K. The results of 500 K nitrogen show greater deviation from the DSMC results indicated by the comparison of residuals. The deviation was due to decreased signal to noise ratio associated with CRBS at 500 K. However, all three sets of results exhibit a line shape narrowing from the published low intensity model. It should be noted that, a complete narrowing was not present as higher frequency differences (greater than 2 GHz and 3.3 GHz for nitrogen at 300 K and 500 K and greater than 2.6 GHz for methane) which yielded results that coincide with the low intensity model. The largest deviations in all three cases occurred at frequency differences corresponding to lattice velocities near the gas most probable speed.

In the low intensity or perturbative regime, the impact on the gas is assumed small and thus has a negligible impact to the thermodynamic state of the gas. However, it has previously been suggested that energy and momentum transfer from the field to the gas can result from high intensity pulsed optical lattices [15, 28]. At higher intensities, changes in the gas state (temperature and bulk motion) may affect the formation of the density grating and therefore the scattering efficiency. Thus, energy and/or momentum transfer from the lattice may contribute to the deviation of the CRBS line shape from low intensity models. This is particularly evident in the energy and momentum transfer calculated by Shneider [15] in air initially at 300 K from a 1 ns optical lattice pulse. The calculations in ref [15] were performed assuming square wave lattice potential wells rather than sinusoidal. This assumption does not represent a practical laser induced optical lattice interaction; however, the presented predictions yield sufficient approximations to a real system. As the potential well depths approach the thermal energy of the gas, trapped molecules transfer energy from the potential field to the bulk medium through collisions.

As indicated in ref [15], the temperature increase and induced bulk motion is highly dependent on the optical lattice velocity. Because the potential well created by an optical lattice tends to flatten the velocity distribution around the lattice velocity, the disturbance to the velocity distribution depends on its derivative [18]. At lattice velocities near the most probable speed, 1/β where $\beta = \sqrt{m/2kT}$, the slope of the distribution is at its maximum, thus causing more significant deviations from equilibrium than those near zero or at the wings. As collisions work to dissipate this perturbation to the distribution, energy is transferred from the lattice to the gas.

In comparing ref [15] to the residual plots in FIG. 4, it can be seen that the deviation from low intensity CRBS line shapes (residual) follows a similar trend as the energy and momentum transfer with lattice velocity. While the peak deviation indicated in the residuals falls closer the peak for momentum transfer (~$1/\sqrt{2}\beta$) rather than energy transfer ($1/\beta$), the trend suggests a gas dynamic phenomenon from the optical lattice-gas interaction instead of other laser-gas interactions such as optically induced ionization or dissociation. This is further supported by agreement between experiment and DSMC, the latter of which only models gas collisional effects.

As further evidence of energy/momentum transfer from the lattice, FIG. 5 shows the numerical sampling of temperature and velocity distribution from the DSMC 300 K nitrogen test. FIG. 5(a) shows the DSMC results for the average gas temperature (centerline) at the end of the laser pulse as a function of lattice phase velocity. The translational and rotational temperature at the end of the pulse are in equilibrium due to the short collision time (~150 ps) compared to the pulse width (~5 ns) of the laser. However, the vibrational temperature remains frozen at this temperature and timescale. Similar plots for nitrogen at 500 K and methane have been generated, but are not shown in the interest of space.

As expected, the temperature profile indicates a dependence on lattice velocity where the peak temperature occurs at a velocity near 1/β. For nitrogen initially at 300 K, subjected a pump intensity of 1.0 x 10^{16} W/m^2, the maximum temperature achieved is 351 K and occurs at a lattice velocity of 450 m/s. This temperature increase is also depicted in FIG. 5(b), which shows the velocity distribution at the beginning and end of the pulse for a lattice velocity of 450 m/s. Also shown is the Maxwellian distribution for the respective gas state. As shown in FIG. 5(b) the velocity distribution reaches thermal equilibrium at the end of the pulse due to the short collision time. Collisions between trapped and untrapped molecules induce a slight bulk motion (~100 m/s) in the direction of the phase velocity; although this flow velocity is significantly lower than the lattice velocity.

VI. CONCLUSION

An experimental and DSMC study was conducted to investigate coherent Rayleigh-Brillouin scattering in high intensity laser fields. The results from the study indicate a narrowing in the CRBS line shape compared to previously published low intensity line shape models. The narrowing can be attributed to the greater impact the optical field has on the gas as the optical potential wells approach the gas thermal energy. In this high intensity regime, molecules are significantly affected by the wells, transferring momentum and energy to the gas through collisions, causing a temperature increase and inducing a bulk flow in the direction of the moving lattice. Comparison between the deviation of high intensity CRBS from low intensity theory and published results for energy and momentum transfer yields similar trends. The variation with optical lattice velocity suggests a gas collisional effect from the optical lattice interaction and not laser induced ionization or dissociation. The DSMC results further support this trend and indicate that nitrogen initially at 300 K can experience a temperature increase of ~51 K and induced bulk flow of ~100 m/s in the presence of a lattice moving at 450 m/s, with a pump intensity of 1.0×10^{16} W/m^2. The energy and momentum transfer from the laser field to the gas resulting from high intensity (near ionization threshold) optical lattices offer a potentially powerful tool for laser based neutral gas heating , acceleration, and flow modification.

ACKNOWLEDGMENTS

The authors wish to recognize and thank Dr. Mikhail Shneider for his patient and beneficial discussions. This work was supported by the Air Force Office of Scientific Research (AFOSR). The authors would like to thank Dr. Mitat Birkan (AFOSR/RSA) for his support of numerical efforts and Dr. Tatjana Curcic (AFOSR/RSE) for her support of experimental efforts. This work was also supported, in part, by a grant of computer time from the DOD High Performance Computing Modernization Program at the U.S. Army Engineer Research and Development Center DoD Supercomputing Resource Center (ERDC DSRC). This work used, in part, the Extreme Science and Engineering Discovery Environment (XSEDE), which is supported by National Science Foundation grant number OCI-1053575.

REFERENCES

1 R. W. Boyd, *Nonlinear Optics* (Academic Press, Inc., San Diego, CA, USA, 2008).

2 H. J. Metcalf and P. Van der Straten, *Laser cooling and trapping* (Springer Verlag, 1999).

3 J. H. Grinstead and P. F. Barker, Physical Review Letters **85**, 1222 (2000).

4 X. Pan, M. N. Shneider, and R. B. Miles, Physical Review Letters **89**, 183001 (2002).

5 G. Tenti, C. D. Boley, and R. C. Desai, Canadian Journal of Physics **52**, 285 (1974).

6 X. Pan, P. F. Barker, Meschanov, A. V., R. B. Miles, and J. H. Grinstead, in *Aerospace Sciences Meeting and Exhibit* (American Institute of Aeronautics and Astronautics, Reno, Nevada, USA, 2001).

7 X. Pan, P. F. Barker, A. Meschanov, M. N. Shneider, and R. B. Miles, Optics Letters **27**, 161 (2002).

8 X. Pan, M. N. Shneider, Z. Zhang, and R. B. Miles, in *AIAA Aerospace Sciences Meeting and Exhibit* (American Institute of Aeronautics and Astronautics, Reno, Nevada, USA, 2004), Vol. 42.

9 A. S. Meijer, A. S. de Wijn, M. F. E. Peters, N. J. Dam, and W. van de Water, Journal of Chemical Physics **133**, 164315 (2010).

10 X. Pan, Ph.D. Dissertation, Princeton University, 2003.

11 H. T. Bookey, M. N. Shneider, and P. F. Barker, Physical Review Letters **99**, 133001 (2007).

12 B. M. Cornella, S. F. Gimelshein, M. N. Shneider, T. C. Lilly, and A. D. Ketsdever, Optics Express **20**, 12975 (2012).

13 B. M. Cornella, S. F. Gimelshein, T. C. Lilly, and A. D. Ketsdever, in *28th International Symposium on Rarefied Gas Dynamics*, edited by M. Mareschal and A. Santos (American Institute of Physics, Zaragoza, Aragon, Spain, 2012).

14 M. N. Shneider and P. F. Barker, Physical Review A **71**, 053403 (2005).

15 M. N. Shneider, P. F. Barker, and S. F. Gimelshein, Applied Physics A **89**, 337 (2007).

16 X. Pan, M. N. Shneider, and R. B. Miles, Physical Review A **69**, 033814 (2004).

17 H. T. Bookey, A. I. Bishop, M. N. Shneider, and P. F. Barker, Journal of Raman Spectroscopy **37**, 655 (2006).

18 M. N. Shneider, P. F. Barker, X. Pan, and R. B. Miles, Optics Communications **239**, 205 (2004).

19 B. M. Cornella, Ph.D. Dissertation, University of Colorado Colorado Springs, 2012.

20 M. O. Vieitez, E. J. van Duijn, W. Ubachs, B. Witschas, A. Meijer, A. S. de Wijn, N. J. Dam, and W. van de Water, Physical Review A **82**, 043836 (2010).

21 T. Lilly, A. Ketsdever, B. Cornella, T. Quiller, and S. Gimelshein, Applied Physics Letters **99**, 124101 (2011).

22 T. C. Lilly, Ph.D. Dissertation, University of Southern California, 2010.

23 G. A. Bird, *Molecular Gas Dynamics and the Direct Simulation of Gas Flows* (Oxford University Press, New York, New York, U.S.A., 1994).

24 M. S. Ivanov and S. V. Rogasinsky, Russian Journal of Numerical Analysis and Mathematical Modelling **3**, 453 (1988).

25 J. G. Parker, Physics of Fluids **2**, 449 (1959).

26 R. C. Millikan and D. R. White, The Journal of Chemical Physics **39**, 3209 (1963).

27 A. Manteghi, N. J. Dam, A. S. Meijer, A. S. de Wijn, and W. van de Water, Physical Review Letters **107**, 173903 (2011).

28 M. N. Shneider, P. F. Barker, and S. F. Gimelshein, Journal of Applied Physics **100**, 074902 (2006).

FIGURES

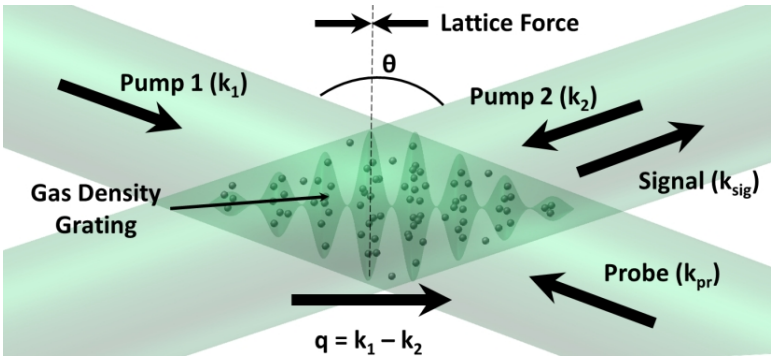

FIG. 1. (Color online) Diagram of test optical phase configuration and gas interaction.

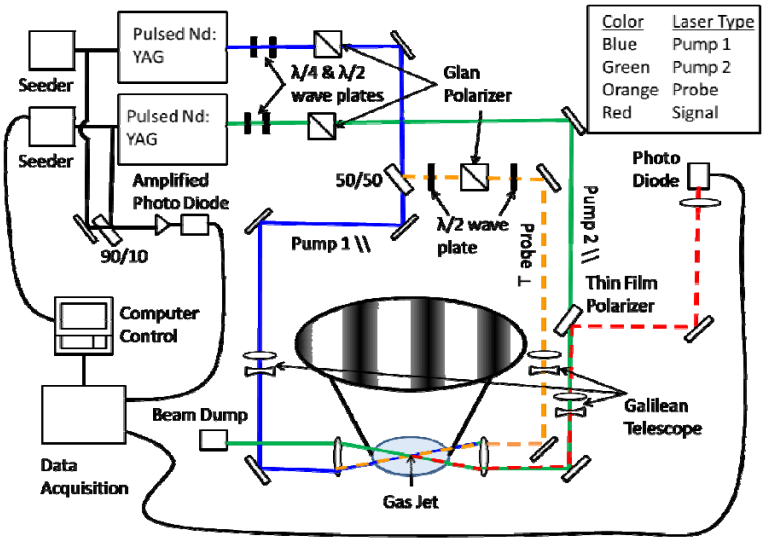

FIG. 2. (Color online) Diagram of test optical configuration.

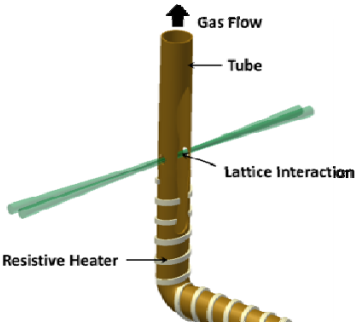

FIG. 3. (Color online) Diagram of test gas configuration.

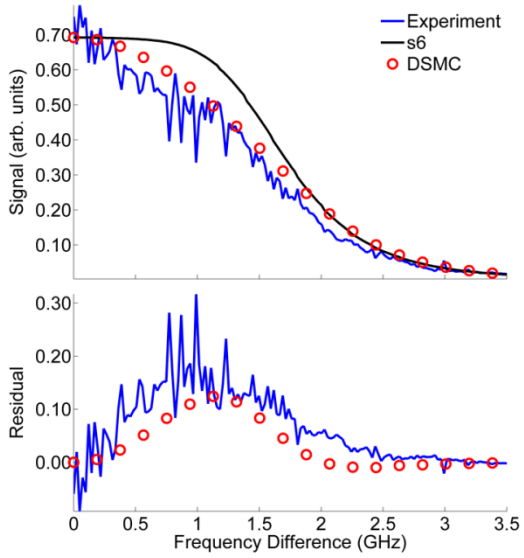
Experiment
s6
DSMC
Signal (arb. units)
0.70
0.60
0.50
0.40
0.30
0.20
0.10
Residual
0.30
0.20
0.10
0.00
0
0.5
1
1.5
2
2.5
3
3.5
Frequency Difference (GHz)

(a)

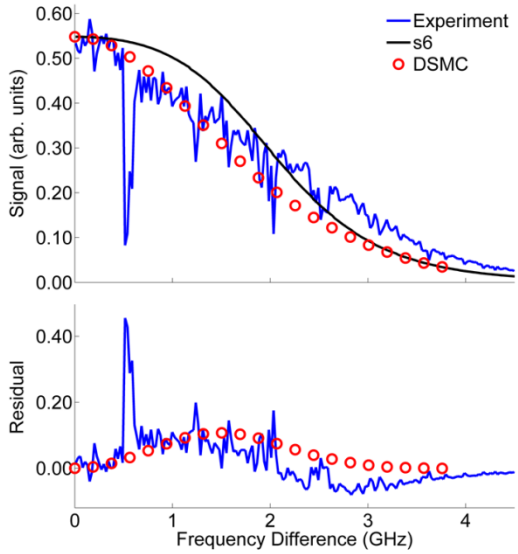
Experiment
s6
DSMC
Signal (arb. units)
0.60
0.50
0.40
0.30
0.20
0.10
0.00
Residual
0.40
0.20
0.00
0
1
2
3
4
Frequency Difference (GHz)

(b)

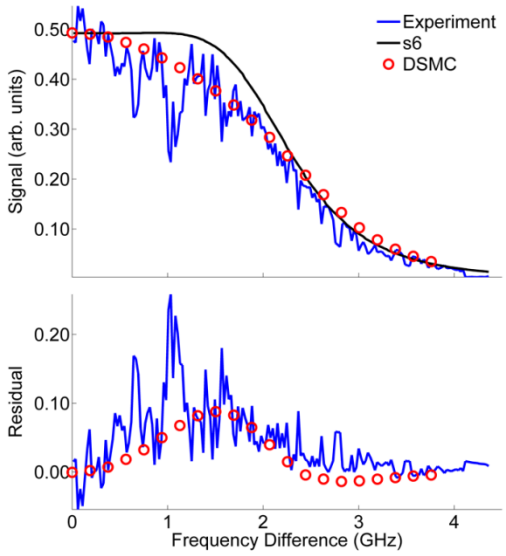

(c)

FIG. 4. (Color online) Comparison of high intensity CRBS line shapes with low intensity model for (a) nitrogen at 300 K (b) nitrogen at 500K and (c) methane at 300 K. The low intensity model is represented by solid black (only upper plot), experimental points are represented by solid blue (both upper and lower plot), and numerical predictions are represented by red circles.

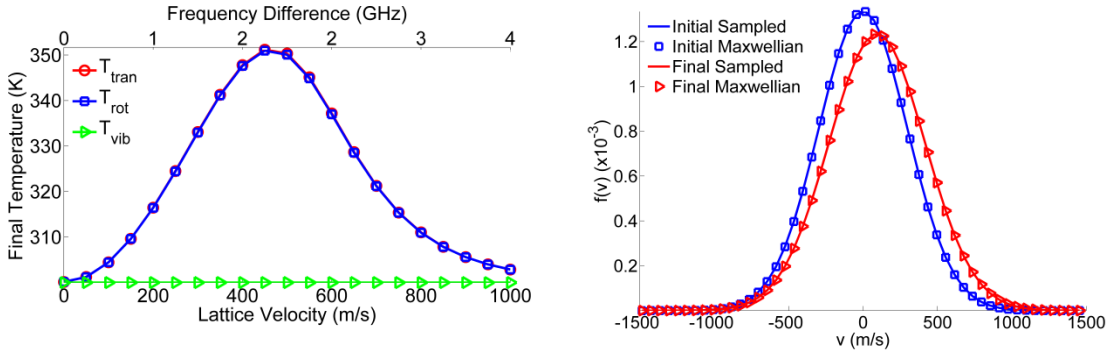

(a) **(b)**

FIG. 5. (Color online) Simulated (a) centerline nitrogen (300 K) temperature as a function of lattice velocity and (b) domain-averaged initial and final velocity distributions for a lattice velocity of 450 m/s. Temperatures are represented by red circles, blue squares, and green triangles for translational, rotational, and vibrational temperatures respectively. Velocity distributions are represented by blue squares and red triangles for initial and final distributions respectively.